Analysis of Ferrite Circulators by 2-D Finite-Element and Recursive Green's Function Techniques

Harvey S. Newman, *Member, IEEE,* and Clifford M. Krowne, *Senior Member, IEEE*

***Abstract*—Ferrite circulator operation is analyzed here by two techniques. The first employs a two-dimensional (2-D) finite-element (FE) technique, using a publicly available FE package. We show how to adapt this code to the solution of the magnetostatic equations and solve for the distribution of internal magnetic field inside a round ferrite puck of finite thickness, and use it to verify existing approximations for the demagnetizing fields. Additionally, the 2-D FE method has also been used to calculate the RF fields and scattering parameters in circulators having noncircular shapes, as well as nonuniform material properties and bias conditions. We have also investigated the field solutions for round circulators, calculated using a recursive Green's function (RGF) technique. This technique allows for radially varying properties in the material or bias fields, and thus accommodates the nonuniform demagnetizing field distribution in finite pucks. A comparison of the results of this technique with experiment is made. We show how the impedance-matching structures attached to the circulator affect the field distributions inside, and present plots of the field distributions as a function of frequency, which provide insight into circulator operation.**

***Index Terms*— Ferrite circulators, finite-element methods, Green's functions, magnetostatics.**

I. Introduction

DESIGN AND development experience for microstrip circulators began in 1965 [1]. Since then, experimental data and the collective experience of the design community has been used to scale devices with frequency and create new designs for various applications. The general procedure employed was to design, fabricate, measure, analyze, and to iterate these steps in order to optimize. Often, several experimental iterations would be needed. Tradeoff studies would be required to satisfy the various design goals of acceptable insertion loss, return loss, dissipation loss, isolation, bandwidth, port impedances, package size, weight, ferrite material, bias magnet, and cost. Recently, the materials growth community has achieved success in the deposition of thin-film ferrites on ceramic substrates [2] and on semiconductors [3]. Potential applications have grown for miniaturized integrated circulators in the military (transmit/receive (T/R) modules, phased-array radar front-ends) and the civilian product areas. It is anticipated that an accurate circulator device design and simulation tool is needed. In 1993, the Defense Advanced Research Projects Agency (DARPA) sponsored the Ferrite Development Consortium (FDC), having among its goals the development and delivery of a variety of contemporary software tools which would aid the process of design. In this paper, we report on the development and application of some of the software tools created by the FDC for use in the design of ferrite circulators. In Section II of this paper, a two-dimensional (2-D) finite-element (FE) software program is applied to the solution of the static and RF fields in ferrite circulators. The program, which solves linear or nonlinear sets of simultaneous partial differential equations in 2-D regions having straight or curved boundaries, is first used to solve for the approximate distribution of the internal static magnetic field in a ferrite disk. The solution to this problem is then used to validate an analytical approximation for the nonuniform field distribution. With knowledge of the internal fields, the results of two methods for the solution of the 2-D RF fields in a circulator are presented and compared in Section III. These field patterns inside the circulator demonstrate the insight that can be gained into circulator operation using analytical techniques.

Manuscript received April 4, 1997; revised November 21, 1997. This work was supported by the Office of Naval Research and the Defense Advanced Research Projects Administration Ferrite Development Consortium.

The authors are with the Microwave Technology Branch, Electronics Science and Technology Division, Naval Research Laboratory, Washington DC 20375 USA.

Publisher Item Identifier S 0018-9480(98)01593-2.

II. Application of 2-D FEM

A. Solution for the Internal Static Magnetic Bias Field

In performing static magnetic-field calculations for circulators, it is often erroneously assumed that the applied magnetic field H_{appl} is uniform over the entire region of the magnetic material. While this status can be satisfactorily approached in laboratory measurements using large electromagnetic pole pieces, the assumption is not valid for a packaged miniaturized circulator with a nonideal geometrical arrangement of ferrite puck, permanent magnet, and flux return path. However, even if the applied magnetic field is maintained uniform, the internal magnetic field H_{int}, which determines the values of the terms in the RF permeability tensor, would still not be uniform, except in the limit of infinitesimal circulator thickness. Instead, the circulator's aspect ratio (radius to height) determines the degree to which the nonuniform demagnetization field opposes the applied magnetic field. A result of this internal bias field variation is that ferromagnetic resonance (FMR), at which the magnetic dissipation losses are a maximum, is spread out over a wide range of frequencies. The conventional thinking for field-below-resonance circulator design has been that the FMR could be placed at zero frequency by using an applied bias field approximately equal to the saturation magnetization. If the demagnetization is not uniform, but varies widely, then in

some cases the static magnetic field and, therefore, the FMR frequency in the outer parts of the circulator puck rises to such a high frequency that it may appear at the low-frequency end of the desired operating frequency range.

The internal dc-bias field can be obtained by a direct solution of Maxwell's magnetostatic (time-independent) equations. Ampere's law governing the magnetic field $\mathbf{H}$ in current-free time-independent conditions is $\nabla \times \mathbf{H} = 0$ and, therefore, $\mathbf{H}$ may equivalently be given by the gradient of a magnetostatic potential Ψ:

$$\mathbf{H} = -\nabla\Psi. \tag{1}$$

For nonlinear ferrite material, $\mathbf{B} = \mu_0(\mathbf{H} + \mathbf{M})$, where $\mathbf{M}$ represents the magnetization inside the material caused by $\mathbf{H}$. If the $\mathbf{B}$–$\mathbf{H}$ relation can be assumed to be single valued (by neglecting the small hysteresis effect close to zero applied field), the magnetic flux density $\mathbf{B}$ is a nonlinear monotonically increasing function of $\mathbf{H}$ and in the same direction as $\mathbf{H}$. The magnetization may be incorporated into a nonlinear permeability term $\mu(H)$, giving

$$\mathbf{B} = \mu(H)\mathbf{H} \tag{2}$$

where H is the magnitude of $\mathbf{H}$. Recalling that $\nabla \cdot \mathbf{B} = 0$, we obtain the nonlinear Poisson equation for the magnetostatic potential

$$\nabla \cdot [\mu(|\nabla\Psi|)\nabla\Psi] = 0 \tag{3}$$

from which the z-directed internal magnetic field may obtained from the gradient

$$H_z = -\frac{\partial\Psi}{\partial z}. \tag{4}$$

This is the internal dc magnetic field used in the 2-D analysis of the circulator.

To solve (3) for circular ferrite pucks, we have employed an established 2-D FE solver named PDE2D [4]. PDE2D solves equations of the form

$$\frac{d}{dx}\mathsf{A}\left(x,y,t,\mathbf{U},\frac{\partial\mathbf{U}}{\partial x},\frac{\partial\mathbf{U}}{\partial y}\right) + \frac{d}{dx}\mathsf{B}\left(x,y,t,\mathbf{U},\frac{\partial\mathbf{U}}{\partial x},\frac{\partial\mathbf{U}}{\partial y}\right) = \mathsf{F}\left(x,y,t,\mathbf{U},\frac{\partial\mathbf{U}}{\partial x},\frac{\partial\mathbf{U}}{\partial y}\right) \tag{5}$$

where A, B, and F may be linear or nonlinear vector functions of the spatial coordinates x and y, of the time t, and of the unknown vector $\mathbf{U}$. The region in which the equations are solved may have straight or curved boundaries, and the boundary function G_1 or G_2 must be specified as either one of two forms: either $\mathsf{A}n_x + \mathsf{B}n_y = \mathsf{G}_1(x,y,t,\mathbf{U})$ (free boundary conditions), or $\mathbf{U} = \mathsf{G}_2(x,y,t)$ (fixed boundary conditions). In these expressions, n_x and n_y are the values of the x and y components of a unit vector outwardly normal to the boundary. If the problem is time dependent or nonlinear, an initial condition or a starting estimate $\mathbf{U} = \mathbf{U}_0(x,y,t)$ must be specified. PDE2D has been applied in the past to a wide variety of problems, and recently to the problem of waveguide propagation [5], [6].

To use PDE2D to solve for the demagnetizing fields in a ferrite puck, the nonlinear Poisson equation must be put into the proper formalism. In polar coordinates, (3) may be written

$$\frac{1}{r}\frac{\partial}{\partial r}(rB_r) + \frac{1}{r}\frac{\partial}{\partial\phi}(B_\phi) + \frac{\partial}{\partial z}(B_z) = 0. \tag{6}$$

The three-dimensional (3-D) circular puck may be analyzed in two dimensions by recognizing that the cylindrical symmetry enforces the absence of a ϕ-varying magnetic field. Equation (6) becomes

$$\frac{1}{r}\frac{\partial}{\partial r}(rB_r) + \frac{\partial}{\partial z}(B_z) = 0. \tag{7}$$

with the components given by

$$B_r = \mu(H)H_r, \quad B_z = \mu(H)H_z \tag{8}$$

from (2).

The $1/r$ leading term in the Poisson equation is a singularity at the origin, so we multiply through by r and combine (1), (7), and (8). We set $\mathbf{U} = U = \Psi$, and identify $x \to r$, $y \to z$, and solve for U and its spatial derivatives. Using subscript notation to represent the r and z derivatives $U_r = \partial U/\partial r$ and $U_z = \partial U/\partial z$, we obtain

$$\frac{\partial}{\partial r}(r\mu(H)U_r) + \frac{\partial}{\partial z}(r\mu(H)U_z) = 0 \tag{9}$$

$$H = \sqrt{U_r^2 + U_z^2} \tag{10}$$

where $\mu(H)$ is given by the B-H relation for the ferrite material.

The 2-D problem is solved for a cylindrical space surrounding the ferrite puck, as shown in Fig. 1. Let the ferrite puck have radius a and thickness $2h$. The cylindrical air space surrounding the puck has a radius of L_r and a height of L_z. Because of symmetry, the problem needs only to be solved for the space $0 \le r \le L_r$ and $0 \le z \le L_z$, which is a quarter of the vertical cut plane through the axis. In this solution region, the ferrite material occupies the space $0 \le r \le a$ and $0 \le z \le h$.

The boundary conditions are applied as follows. If the entire solution space is immersed in a uniform z-directed applied magnetic field in the absence of the ferrite puck, then $H_{\text{applied}} = -dU/dz$ on the upper boundary of the space, far from the puck. At $r = 0$ and at $r = L_r$, $H_r = 0$ since there are no radially directed magnetic fields here. At the lower boundary (the midplane of the puck), the magnetostatic potential may be defined to be zero, since by symmetry the fields are normal to the $z = 0$ line.

The permeability function $\mu(H)$ is defined as follows. Outside the puck, $\mu(H) = \mu_0$. Inside the puck, we require that the permeability function must be single valued, so hysteresis is neglected. A reasonable and convenient analytic approximation developed here for the permeability function of a ferrite is

$$\mathbf{B} = \mu(H)\mathbf{H} = \mu_0\left(1 + \frac{M_s}{\sqrt{H_1^2 + H^2}}\right)\mathbf{H}. \tag{11}$$

Here, M_s is the saturation magnetization and H_1 is the "corner" magnetic field at which the magnetization reaches

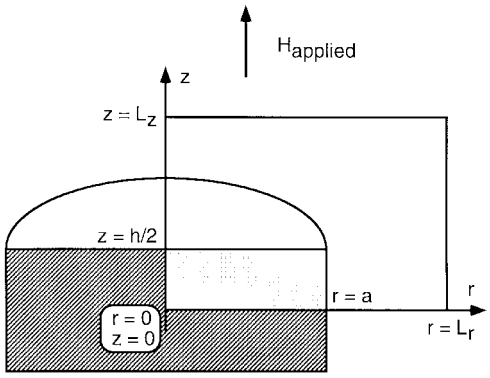

Fig. 1. Cross section of the ferrite puck showing the solution space for the 2-D FE solution for the internal magnetic field. The solution is obtained in the region $0 \leq r \leq a$ and $0 \leq z \leq h$. The ferrite occupies the lower inside portion of this region.

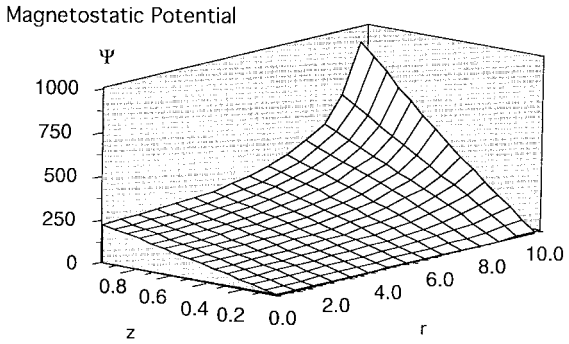

Fig. 2. Plot of the magnetostatic potential Ψ (arbitrary units) for a puck calculated with the 2-D FE solver. The solution space shown corresponds to the quarter-plane region of the cut plane shown in Fig. 1. The magnetic field is the gradient of this potential. Close to the origin, the z-directed magnetic field H_z is relatively constant and increases as the outer wall or top edge of the puck is approached. Fig. 3(a) shows H_z versus r/a.

0.707 times its saturation value. The asymptotic behavior of this function may be seen to be correct by noticing the asymptotic behavior in the low and high magnetic-field limits. At very low fields, the magnetization is proportional to H and in the same direction as $\mathbf{H}$. At very high fields, the magnetization saturates at M_s, after which the magnetic flux density $\mathbf{B}$ continues to increase at the saturated rate with increasing $\mathbf{H}$, $\mathbf{B} = \mu_0(\mathbf{H}+\mathbf{M}_s)$. By examining $B(H)$ curves for various ferrites [7], we note that the corner field H_1, is often on the order of 1 Oe (in CGS units) and that at that field, the flux density B is on the order of, but still much less than, the saturation magnetization, which is often on the order of thousands of gauss. The advantage of this ferrite model for use in PDE2D over, for example, a piecewise linear model, in which $\mathbf{B} = \mu_0\mu_r\mathbf{H}$ for $H < H_1$ (μ_r is a relative permeability) and $\mathbf{B} = \mu_0(\mathbf{H}+\mathbf{M}_s)$ for $H > H_1$ is that the Jacobian matrix elements are continuous and may be calculated explicitly. The Jacobian matrix for this PDE is

$$J = \begin{bmatrix} \frac{\partial \mathsf{F}}{\partial U} & \frac{\partial \mathsf{F}}{\partial U_r} & \frac{\partial \mathsf{F}}{\partial U_z} \\ \frac{\partial \mathsf{A}}{\partial U} & \frac{\partial \mathsf{A}}{\partial U_r} & \frac{\partial \mathsf{A}}{\partial U_z} \\ \frac{\partial \mathsf{B}}{\partial U} & \frac{\partial \mathsf{B}}{\partial U_r} & \frac{\partial \mathsf{B}}{\partial U_z} \end{bmatrix} = -\begin{bmatrix} 0 & 0 & 0 \\ 0 & \frac{\partial \mathsf{A}}{\partial H_r} & \frac{\partial \mathsf{A}}{\partial H_z} \\ 0 & \frac{\partial \mathsf{B}}{\partial H_r} & \frac{\partial \mathsf{B}}{\partial H_z} \end{bmatrix}. \tag{12}$$

Derivatives in (12) are calculated for this ferrite model as

$$\frac{\partial \mathsf{A}}{\partial H_r} = r\left[1 - p - p\frac{H_r^2}{H_1^2 + H^2}\right] \tag{13a}$$

$$\frac{\partial \mathsf{B}}{\partial H_r} = -rp\frac{H_r H_z}{H_1^2 + H^2} \tag{13b}$$

$$\frac{\partial \mathsf{A}}{\partial H_z} = -rp\frac{H_r H_z}{H_1^2 + H^2} \tag{13c}$$

and

$$\frac{\partial \mathsf{B}}{\partial H_z} = r\left[1 - p - p\frac{H_z^2}{H_1^2 + H^2}\right] \tag{13d}$$

in which

$$p = \frac{4\pi M_s}{\sqrt{H_1^2 + H^2}}. \tag{14}$$

Because of the symmetry of the Jacobian matrix, the execution time and the memory storage requirements of the solver are cut in half. The solution is started by assuming an initial guess for the potential given by $U_0(r,z) = -H_{\text{applied}}Z$, which corresponds to the solution in empty space.

The triangulation is chosen by specifying an initial minimum triangulation grid, which uniquely defines the regions of ferrite and air. The triangulation mesh density is then increased proportionately to the gradient of the solution. With the input data for a typical ferrite puck, the problem converges in about ten iterations. The magnetostatic potential Ψ obtained in this manner for a ferrite puck having a diameter-to-height ratio of 10, a saturation magnetization of 2000 G, in an applied magnetic field of 2000 Oe, is shown in Fig. 2. H_z corresponding to Ψ at the midplane of the puck is provided in Fig. 3(a).

We have found that the approximation by Joseph and Schloemann (JS approximation) [8], agrees well with the more exact 2-D FE solution and we have incorporated their approximation into the 2-D circulator solution. The JS approximation calculates the value of the demagnetization factor N_{zz} for use in the demagnetization equation for the internal dc magnetic field

$$H_{\text{int}} = H_{\text{appl}} - N_{zz}4\pi M_s. \tag{15}$$

In the limit of an infinitesimally thin film, $N_{zz} = 1$, and H_{int} can be made equal to zero by setting $H_{\text{appl}} = 4\pi M_s$. For pucks of finite thickness, N_{zz} is a function of radial and vertical position. Fig. 3(b) shows N_{zz} given by the JS approximation compared with the effective N_{zz} obtained by the 2-D FE method used above, calculated at the midplane of the puck for a couple of representative aspect ratios. Results indicate that the JS analytical expansion is a good approximation to the actual internal field for thin circular pucks.

B. Calculation of RF Fields Inside Circulator

It is common practice to bias a circulator with H_{int} close to 0 Oe so the operating frequency may be placed reasonably far from the FMR frequency, and thus the magnetic losses

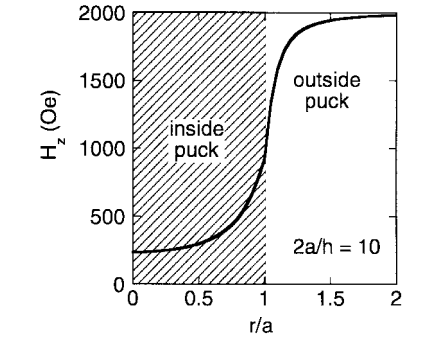

(a)

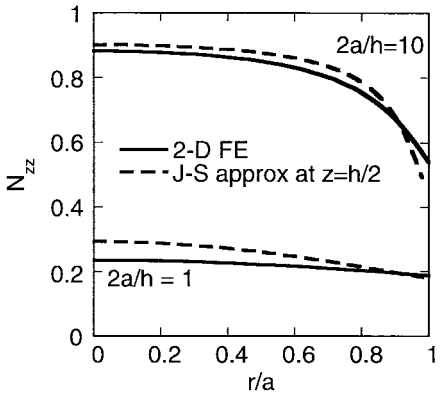

(b)

Fig. 3. (a) Plot of the static magnetic field H_z in a ferrite puck calculated by the 2-D FE code at the horizontal midplane of the puck. (b) Comparison of the equivalent demagnetization factor N_{zz} obtained from this field distribution with the JS approximation. The ferrite is modeled by the $\mathbf{B}$–$\mathbf{H}$ curve of (11), with $4\pi M_s = 2000$ G and the corner magnetic field H_1 equal to 1 Oe.

may be minimized. The FMR frequency is $f_0 = \omega_0/(2\pi) = \gamma H_{\text{int}}$, where γ is the gyromagnetic ratio of approximately 2.8 MHz/Oe. A constant zero value for ω_0 cannot be maintained at every point in the puck, as long as any one or all of the quantities H_{appl}, N_{zz}, and $4\pi M_s$ vary with radial position, except for some extraordinary magnet design for which each of the radial dependencies essentially cancel each other. In practice, therefore, the internal field in the ferrite puck will always vary radially, even though the applied field and the saturation magnetization may be maintained constant. Because the internal magnetic field is a function of radial position, the permeability tensor elements will also be a function of radial position. The 2-D analytical methods previously created to solve the thin round circulator [9] are not valid for a circulator whose properties are not uniform. In the following sections, we will show results of the 2-D FE solver applied to the circulator and compare them to contemporary analytical and Green's function methods for obtaining the fields in a circulator [10].

The analysis of the circulator using the 2-D FE solver begins with the definition of the RF permeability tensor in rectangular coordinates. Assuming that the ferrite material is biased by an applied magnetic field in the z-direction, the RF permeability tensor takes on the form [11]

$$\hat{\mu} = \mu_0 \begin{bmatrix} \mu & -j\kappa & 0 \\ j\kappa & \mu & 0 \\ 0 & 0 & 1 \end{bmatrix} \tag{16}$$

where

$$\mu = 1 + \frac{\omega_m(\omega_0 + j\omega\alpha)}{(\omega_0 + j\omega\alpha)^2 - \omega^2} \tag{17}$$

and

$$\kappa = \frac{\omega_m \omega}{(\omega_0 + j\omega\alpha)^2 - \omega^2}. \tag{18}$$

Here, ω_m is the magnetization frequency given by $\omega_m/(2\pi) = \gamma M_s$, and ω_0 is the ferromagnetic resonant frequency defined earlier. The values of κ and μ may depend upon position. The constitutive relation between the RF magnetic flux density $\mathbf{B}$ and the RF magnetic field $\mathbf{H}$ is thus

$$\mathbf{B} = \hat{\mu} \cdot \mathbf{H} = \mu_0 \begin{bmatrix} \mu H_x - j\kappa H_y \\ j\kappa H_x + \mu H_y \\ H_z \end{bmatrix}. \tag{19}$$

Magnetic losses are included by allowing the ferromagnetic resonant frequency to be complex with loss component α. The constitutive relation between the electric flux density $\mathbf{D}$ and the electric field $\mathbf{E}$ is $\mathbf{D} = \varepsilon\mathbf{E} = \varepsilon_0\varepsilon_r(1 - j\tan\delta)\mathbf{E}$, where dielectric losses are accounted for through the loss tangent δ.

Now, Maxwell's equations in rectangular coordinates are

$$\frac{\partial E_z}{\partial y} - \frac{\partial E_y}{\partial z} + j\omega\mu_0(\mu H_x - j\kappa H_y) = 0 \tag{20a}$$

$$\frac{\partial E_x}{\partial z} - \frac{\partial E_z}{\partial x} + j\omega\mu_0(j\kappa H_x + \mu H_y) = 0 \tag{20b}$$

$$\frac{\partial E_y}{\partial x} - \frac{\partial E_x}{\partial y} + j\omega\mu_0 H_z = 0 \tag{20c}$$

$$\frac{\partial H_z}{\partial y} - \frac{\partial H_y}{\partial z} - j\omega\varepsilon E_x = 0 \tag{20d}$$

$$\frac{\partial H_x}{\partial z} - \frac{\partial H_z}{\partial x} - j\omega\varepsilon E_y = 0 \tag{20e}$$

$$\frac{\partial H_y}{\partial x} - \frac{\partial H_x}{\partial y} - j\omega\varepsilon E_z = 0. \tag{20f}$$

If we restrict consideration to the 2-D case for which $E_x = E_y = H_z = 0$, and $\partial/\partial z = 0$, then

$$\begin{bmatrix} j\omega\mu_0\mu & \omega\mu_0\kappa & \frac{\partial}{\partial y} \\ \omega\mu_0\kappa & -j\omega\mu_0\mu & \frac{\partial}{\partial x} \\ \frac{\partial}{\partial y} & -\frac{\partial}{\partial x} & j\omega\varepsilon \end{bmatrix} \begin{bmatrix} H_x \\ H_y \\ E_z \end{bmatrix} = 0. \tag{21}$$

These are three linear partial differential equations which can be solved using PDE2D. We normalize the equations by defining

$$\begin{gathered} U_1 = \eta H_x \quad U_2 = \eta H_y \quad U_3 = E_z \\ x' = \frac{x}{a} \quad \text{and} \quad y' = \frac{y}{a} \end{gathered} \tag{22}$$

where a and η are chosen to simplify the equations. Then, setting a equal to the ferrite puck radius, $\eta = \sqrt{\mu_0/(\varepsilon_0\varepsilon_r)}$, and k_0 equal to the propagation constant in the unmagnetized ferrite $k_0 = \omega\sqrt{\mu_0\varepsilon_0\varepsilon_r}$, we obtain

$$\begin{bmatrix} j\mu k_0 a & \kappa k_0 a & \frac{\partial}{\partial y'} \\ \kappa k_0 a & -j\mu k_0 a & \frac{\partial}{\partial x'} \\ \frac{\partial}{\partial y'} & \frac{\partial}{\partial x'} & jk_0 a(1 - j\tan\delta) \end{bmatrix} \begin{bmatrix} U_1 \\ U_2 \\ U_3 \end{bmatrix} = 0. \tag{23}$$

Next, we allow for complex (phasor) fields, and proceed to split the system into real and imaginary parts. The system of equations can be written as

$$\begin{bmatrix} (p_1+jq_1) & (p_2+jq_2) & \frac{\partial}{\partial y'} \\ (p_2+jq_2) & -(p_1+jq_1) & \frac{\partial}{\partial x'} \\ \frac{\partial}{\partial y'} & -\frac{\partial}{\partial x'} & (p_3+jq_3) \end{bmatrix} \begin{bmatrix} u_1+jv_1 \\ u_2+jv_2 \\ u_3+jv_3 \end{bmatrix} = 0 \tag{24}$$

where

$$\begin{aligned} &U_1 = u_1 + jv_1 \quad u_1 = \mathrm{Re}[\eta H_x] \quad v_1 = \mathrm{Im}[\eta H_x] \\ &U_2 = u_2 + jv_2 \quad u_2 = \mathrm{Re}[\eta H_y] \quad v_2 = \mathrm{Im}[\eta H_y] \\ &U_3 = u_3 + jv_3 \quad u_3 = \mathrm{Re}[E_z] \quad\ \ v_1 = \mathrm{Im}[E_z] \\ &p_1 = \mathrm{Re}[j\mu k_0 a] \qquad\qquad q_1 = \mathrm{Im}[j\mu k_0 a] \\ &p_2 = \mathrm{Re}[\kappa k_0 a] \qquad\qquad q_2 = \mathrm{Im}[\kappa k_0 a] \\ &p_3 = \mathrm{Re}[jk_0 a(1-j\tan\delta)] \quad q_3 = \mathrm{Im}[jk_0 a(1-j\tan\delta)]. \end{aligned} \tag{25}$$

Equation (24) may be seen as the following six first-order linear partial differential equations for $\mathbf{U} = \{u_1, u_2, u_3, v_1, v_2, v_3\}$ where, here, the x and y subscripts indicate differentiation by the subscripted variable

$$\begin{aligned} u_{3y} + p_1u_1 - q_1v_1 + p_2u_2 - q_2v_2 &= \mathsf{F}_1 = 0 \\ v_{3y} + q_1u_1 + p_1v_1 + q_2u_2 + p_2v_2 &= \mathsf{F}_2 = 0 \\ u_{3x} + p_2u_1 - q_2v_1 - p_1u_2 + q_1v_2 &= \mathsf{F}_3 = 0 \\ v_{3x} + q_2v_1 + p_2v_1 - q_1u_2 - p_1v_2 &= \mathsf{F}_4 = 0 \\ u_{1y} - u_{2x} + p_3u_3 - q_3v_3 &= \mathsf{F}_5 = 0 \\ v_{1y} - v_{2x} + q_3u_3 + p_3v_3 &= \mathsf{F}_6 = 0. \end{aligned} \tag{26}$$

This set of six partial differential equations fits into the required PDE2D formalism by setting $\mathsf{A} = 0, \mathsf{B} = 0$, and $\mathsf{F}(x, y, t, \mathbf{U}, \mathbf{U}_x, \mathbf{U}_y) = 0$.

The boundary conditions at the ferrite circulator perimeter are of two types. At the boundary corresponding to the ferrite-dielectric wall, a perfect magnetic-wall boundary condition is used. At a wall location whose angle is ϕ, the tangential magnetic field is thus given by

$$H_{\text{tangential}} = H_y\cos(\phi) - H_x\sin(\phi) = 0. \tag{27}$$

The boundary function is $\mathsf{A}n_x + \mathsf{B}n_y = \mathsf{G}_1$. Since both A and B are 0, the boundary function G_1 can be used to enforce the tangential condition

$$\mathsf{G}_1(x, y, t, \mathbf{U}, \mathbf{U}_x, \mathbf{U}_y) = \begin{bmatrix} u_2\cos(\phi) - u_1\sin(\phi) \\ v_2\cos(\phi) - v_1\sin(\phi) \end{bmatrix} = \begin{bmatrix} 0 \\ 0 \end{bmatrix} \tag{28}$$

which makes both the real and imaginary parts of the tangential (to the cylindrical wall) magnetic field, located at the angle ϕ, equal to 0. At the ports, a field matching boundary condition is implemented. At port 1, the incident port, the z-directed electric field at the port boundary is asserted to have unit amplitude and zero phase, so $\mathrm{Re}[E_z] = E_0 = 1$ and $\mathrm{Im}[E_z] = 0$. The tangential magnetic field, which is continuous across the port interface, is matched to the tangential magnetic field in the outside dielectric, which is given by the electric field divided by the wave impedance in the outside dielectric

$$H_{\text{tangential}} = H_y\cos(\phi) - H_x\sin(\phi) = E_0/\eta_d. \tag{29}$$

This leads us to the boundary function for port 1:

$$\begin{aligned} &\mathsf{G}_1(x, y, t, \mathbf{U}, \mathbf{U}_x, \mathbf{U}_y) \\ &\quad = \begin{bmatrix} u_2\cos(\phi) - u_1\sin(\phi) - \frac{\eta}{\eta_d}E_0 \\ v_2\cos(\phi) - v_1\sin(\phi) \end{bmatrix} = \begin{bmatrix} 0 \\ 0 \end{bmatrix}. \end{aligned} \tag{30}$$

At the forward transmission and isolated ports (ports 2 and 3) the field is not specified as at port 1, but the ratio of the fields is equal to the wave impedance in the dielectric

$$H_{\text{tangential}} = H_y\cos(\phi) - H_x\sin(\phi) = E_z/\eta_d \tag{31}$$

giving at ports 2 and 3

$$\begin{aligned} &\mathsf{G}_1(x, y, t, \mathbf{U}, \mathbf{U}_x, \mathbf{U}_y) \\ &\quad = \begin{bmatrix} u_2\cos(\phi) - u_1\sin(\phi) - \frac{\eta}{\eta_d}u_3 \\ v_2\cos(\phi) - v_1\sin(\phi) - \frac{\eta}{\eta_d}v_3 \end{bmatrix} = \begin{bmatrix} 0 \\ 0 \end{bmatrix}. \end{aligned} \tag{32}$$

These boundary conditions are similar to those used by Bosma in his original solution [9]. Equation (26), with the boundary conditions of (28), (30) and (32), provides the required set of equations to solve the problem.

The numerical procedure outlined above was used to analyze an embedded puck circulator (a ferrite puck surrounded by dielectric) and the results compared with previously published Green's function analytical codes for uniform circulators [12], [13]. For a sufficiently small triangulation grid (Fig. 4) which yields smooth plotted results, the calculation time on a high-end workstation is a couple of minutes per frequency point. The 2-D FE code, though considerably slower than the analytical solution (which typically requires only a few seconds per frequency point), is valuable not only in solving arbitrarily shaped noncircular 2-D problems, but also by providing insight and a validity check for the analytical code. Fig. 5 exhibits the agreement between the 2-D FE solver and the analytical code for a round circulator. The S-parameter results obtained from the 2-D FE code closely match the analytical results. Fig. 6(a) exhibits the electric-field standing wave pattern in the circulator, assuming the intrinsic matching conditions described above.

A particular advantage of the 2-D FE approach is that it can be applied to arbitrary geometries, for which the analytical codes based on circular basis functions cannot be applied, and inhomogeneous material or inhomogeneous bias conditions. An example of these calculations for a hexagonally shaped

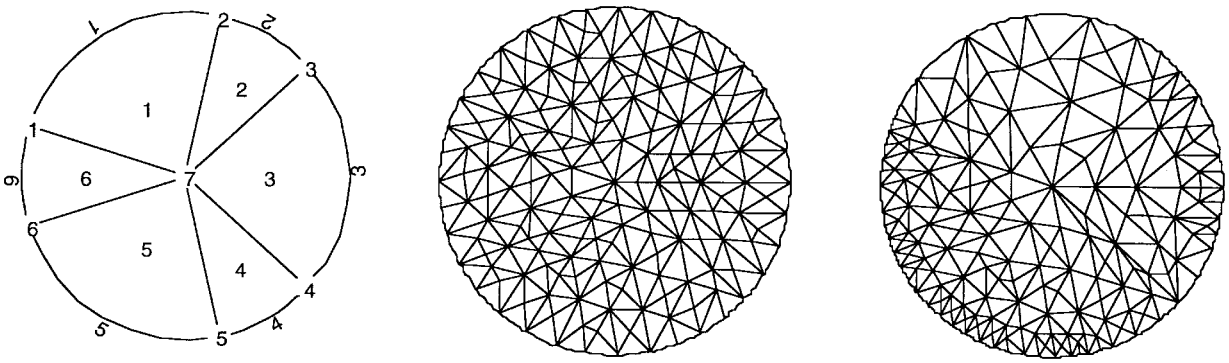

Fig. 4. Triangulation grids used by the 2-D FE code. (a) Initial triangulation pattern defined at the start of the simulation. The seven vertices, six triangles (generalized to have curved or straight boundaries), and six boundary arcs are labeled. The transmission lines, which adjoin the disk at arcs 2, 4, and 6, are not shown. (b) Final triangulation (300 triangles) produced by the 2-D FE code. (c) Final triangulation after adaptive refinement. Here, the triangulation pattern of (b) was modified to densify the triangles in regions where the solution had the highest gradient.

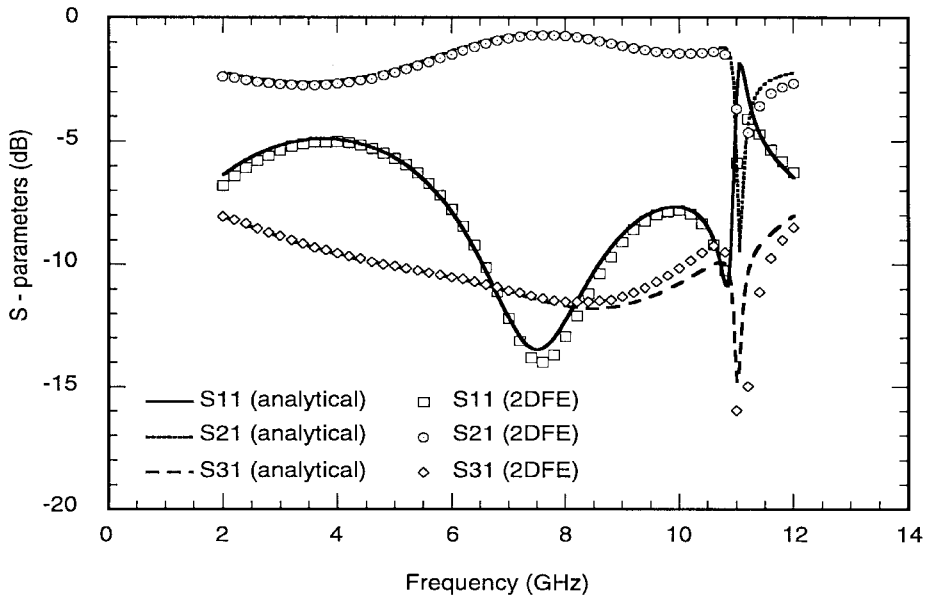

Fig. 5. Comparison of the S-parameters of an embedded puck circulator, calculated by the 2-D FE method with the analytical solution, showing excellent agreement. The calculation is made for an intrinsic circulator, i.e., one which has a signal incident on port 1, with only outgoing signals at ports 2 and 3. The calculations assumed that the ferrite was YIG with a $4\pi M_s = 1780$ G, $\varepsilon_r = 15$ for both the ferrite and the outside dielectric, a loss tangent of 0.0002, and a linewidth $\Delta H = 45$ Oe. The external bias field was 1780 Oe, and the variation of the demagnetization fields over the puck and the anisotropy fields were neglected in both calculations. The circulator had a port aperture width $= 1.5$ mm, puck radius $= 2.79$ mm, and the puck height $= 0.508$ mm.

circulator is shown in Fig. 6(b). Here, the noncircular shape is chosen to be a threefold symmetric six-sided structure. The internal magnetic field is assumed uniform and demagnetization is neglected. The contours in the plot are contours of constant magnitude of the z-directed electric field, illustrative of the standing wave in the ferrite resonator. The material parameters and magnetic bias were identical to that of the round circulator of Fig. 6(a), only the shape was changed, keeping the major radius of the two devices the same.

III. Application of the 2-D Recursive Green's Function Solver

For the important special case of round circulators having radially varying nonuniformity, Green's function techniques have been recently extended to handle radial variation. To solve the circulator analytically in the presence of radial variation, we have previously developed a recursive Green's function (RGF) solution [10] as opposed to the use of a single uniform region Green's function [12], [13]. The theory behind the RGF allows many of the efficient economies of the Green's function theory to be applied to the evaluation of the RGF. This leads to extremely short calculation times compared to that found for numerically intensive simulators like finite-difference and FE codes. The essence of the RGF approach is to break up the circulator puck into a single internal disk containing the origin and a set of concentric annuli or rings. Each of these circulator zones may be characterized by different values of applied magnetic bias field, saturation magnetization, and demagnetization factor. In this way, the circulator, with natural as well as intentionally imposed inhomogeneities, can be properly modeled. The RGF theory applied to circulators

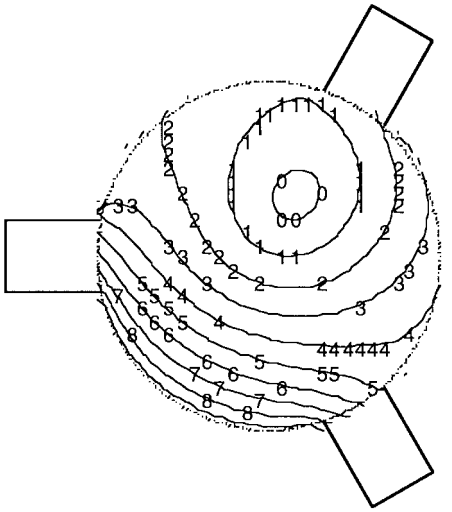

(a)

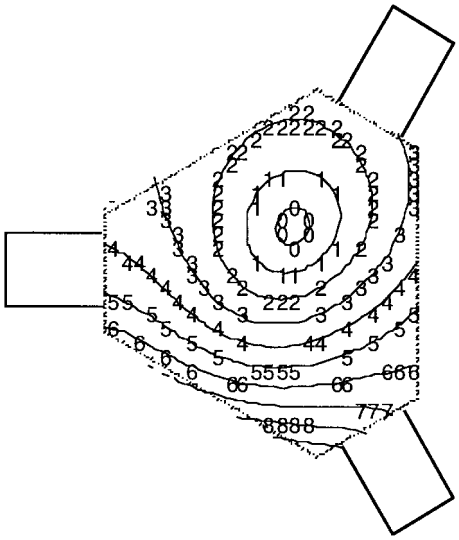

(b)

Fig. 6. Contours of constant electric-field magnitude in an intrinsically matched (a) round circulator and (b) "hexagonal" circulator, as calculated by the 2-D FE code. The higher index numbers which label the contours correspond to higher magnitudes of the vertical electric field. The input port is at the left, the isolated port is at the upper right. The frequency is close to the frequency of maximum isolation. Both devices were calculated assuming uniform $4\pi M_s = 2300$ G, and $H_{\text{applied}} = 2300$ Oe, and $\Delta H = 320$ Oe. The ferrite dielectric constant is 13.3, the outer dielectric constant is 9.5, and the ferrite loss tangent is 0.0003. The radius of the round puck is 2.7026 mm, the height is 0.635 mm, and the port aperture is 1.67 mm. The "hexagonal" circulator had all material parameters the same as the round circulator, and was of the same thickness. The major diameters and the port apertures of both devices were the same, and the sidewalls containing the ports on device (b) were each 1.7 mm.

has been thoroughly presented in [14] and [15]. This capability to account for radial variations can provide new insight. In this section we will present some applications and new results of the RGF solution.

Consider the "ringed" circulator shown in Fig. 7. Consider first the case for which the ferrite is uniform and the rings are used simply to provide a way of allowing the internal field in the rings to vary radially. This corresponds to the case when the demagnetizing factor is the only radially

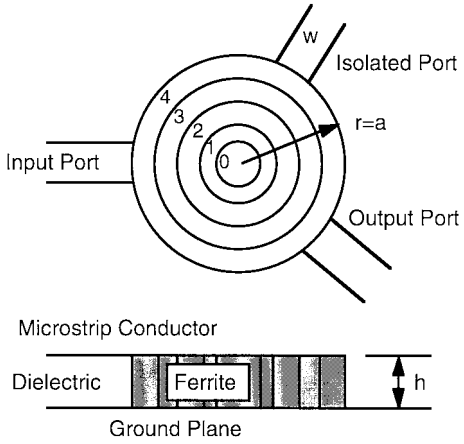

Fig. 7. Diagram of a radially varying circulator which shows how the region is broken up into concentric rings. Each ring is assumed to have constant saturation magnetization and applied magnetic field.

varying parameter. Using the JS approximation, $N_{zz}(r)$ can be calculated. From the prior discussion it is obvious how radial variations in the externally applied bias field, or in the saturation magnetization, can be treated, once the ringed circulator analysis capability is in place. Circulators having multiple rings of different ferrite materials can be readily analyzed, as well as those with a combination of ferrite and dielectric rings. To model a dielectric ring it is only necessary to assign it a saturation magnetization of zero, which takes away all magnetic properties while leaving its dielectric properties intact.

In the RGF technique, an algorithm for calculating the dyadic Green's functions for a ferrite puck is implemented. The Green's functions are kernels which relate the electric field at a particular point (the response point) to the magnetic fields on the boundary (the source point). It is important to realize that the dyadic Green's functions can be obtained without knowledge of the outside circuits or transmission lines. This technique only requires a specification of the source fields (the magnetic fields) at the boundary. Since the magnetic-wall condition ($H_\phi = 0$ at $r = a$, if $\phi \neq \phi_i$) is assumed to hold everywhere except at the ports, then the only source points are at the ports.

If the ports are labeled 1, 2, and 3, then the electric field at any point in the interior of the ferrite disk is given by

$$E(r,\phi) = G_1(r,\phi)H_1 + G_2(r,\phi)H_2 + G_3(r,\phi)H_3. \quad (33)$$

Also, when the response point is at the ports the electric field can be expressed as

$$\begin{pmatrix} E_1 \\ E_2 \\ E_3 \end{pmatrix} = \begin{bmatrix} G_{11} & G_{12} & G_{13} \\ G_{21} & G_{22} & G_{23} \\ G_{31} & G_{32} & G_{33} \end{bmatrix} \begin{pmatrix} H_1 \\ H_2 \\ H_3 \end{pmatrix}. \quad (34)$$

In this notation, the Green's function G_{ij} gives the electric field at port i caused by a magnetic field at port j, and the total field is obtained by superposition. All the G_i's and G_{ij}'s in (33) and (34) are calculated in the RGF technique.

We will attach to each of the ports an impedance equal to the wave impedance η_d of a microstrip having a width and height equal to the port width and height and a dielectric

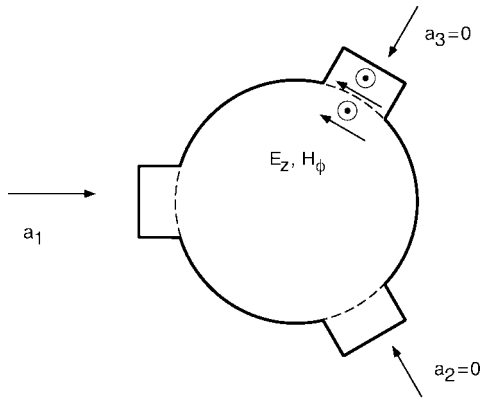

Fig. 8. Signal definitions for the intrinsic circulator. The incident signal appears at port 1, the output signal at port 2, and the isolated signal at port 3. There are no incoming signals at ports 2 and 3.

whose permittivity is chosen by the user. The electric and magnetic fields tangent to the interface between the circulator and the attached microstrip are continuous. The characteristic impedance of the transmission line is proportional to the wave impedance in the transmission line, for TEM and quasi-TEM lines. Therefore, at each port

$$E_{\tan}^{\text{inside}} = E_{\tan}^{\text{outside}} \tag{35a}$$

$$H_{\tan}^{\text{inside}} = H_{\tan}^{\text{outside}} \tag{35b}$$

$$Z_{\text{in}} = \text{constant} \times \eta_{\text{in}} = \text{constant} \times \frac{E_{\tan}^{\text{inside}}}{H_{\tan}^{\text{inside}}} \tag{35c}$$

$$Z_0 = \text{constant} \times \eta_d = \text{constant} \times \frac{E_{\tan}^{\text{outside}}}{H_{\tan}^{\text{outside}}}. \tag{35d}$$

Because the port aperture is the same (obviously) whether you are looking inward to the circulator or outward to the attached microstrip, the proportionality constant relating characteristic impedance to wave impedance is the same in both directions.

The intrinsic circulator's port boundary conditions used here are that at ports 2 and 3 the incident wave amplitude is zero (Fig. 8). This can be accomplished by terminating the attached transmission line in an infinitely absorbing load, so that whatever power does get transmitted into the output lines will never be reflected back into the circulator. It is not the same as an impedance match to the circulator, which would imply maximum power transfer into the transmission lines across the interface and could only be accomplished with a frequency-dependent complex characteristic impedance whose value is the complex conjugate of Z_{in}.

A. Solving for S-Parameters

Let us assume reflectionless load condition at ports 2 and 3, but allow an incoming signal at port 1. For the traveling waves, η_d is equal to the E/H ratio in the microstrip

$$\frac{E_1^{\text{inc}}}{H_1^{\text{inc}}} = \eta_d \tag{36a}$$

$$\frac{E_2^{\text{out}}}{H_2^{\text{out}}} = -\eta_d \tag{36b}$$

$$\frac{E_3^{\text{out}}}{H_3^{\text{out}}} = -\eta_d. \tag{36c}$$

Then we can express all of the port fields in terms of the S-parameters and the amplitude of an incident electric field at port 1

$$E_1 = E_1^{\text{inc}} + E_1^{\text{out}} = E_1^{\text{inc}} + S_{11}E_1^{\text{inc}} = (1 + S_{11})E_1^{\text{inc}} \tag{37a}$$

$$H_1 = H_1^{\text{inc}} - H_1^{\text{out}} = H_1^{\text{inc}} - S_{11}H_1^{\text{inc}} = (1 - S_{11})H_1^{\text{inc}} = \frac{(1 - S_{11})}{\eta_d}E_1^{\text{inc}} \tag{37b}$$

$$E_2 = E_2^{\text{out}} = S_{21}E_1^{\text{inc}} \tag{37c}$$

$$H_2 = H_2^{\text{out}} = -\frac{S_{21}}{\eta_d}E_1^{\text{inc}} \tag{37d}$$

$$E_3 = E_3^{\text{out}} = S_{31}E_1^{\text{inc}} \tag{37e}$$

$$H_3 = H_3^{\text{out}} = -\frac{S_{31}}{\eta_d}E_1^{\text{inc}}. \tag{37f}$$

These six equations [(37a)–(37f)] can be solved for E_1, E_2, and E_3 in terms of H_1, H_2, and H_3. It is found that

$$E_1 = 2E_1^{\text{inc}} - \eta_d H_1 \tag{38a}$$

$$E_2 = -\eta_d H_2 \tag{38b}$$

$$E_3 = -\eta_d H_3. \tag{38c}$$

The electric fields E_1, E_2, and E_3 are then substituted into (34) and the three magnetic fields H_1, H_2, and H_3 are obtained. Returning to (37a) and (37b), the input reflection coefficient is determined as

$$S_{11} = 1 - \eta_d \frac{H_1}{E_1^{\text{inc}}} \tag{39a}$$

and using (37d) and (37f) the transmission coefficients are found as

$$S_{21} = -\eta_d \frac{H_2}{E_1^{\text{inc}}} \tag{39b}$$

$$S_{31} = -\eta_d \frac{H_3}{E_1^{\text{inc}}}. \tag{39c}$$

This solution may be called the "intrinsic" solution for the circulator. It is neither perfectly matched, nor matched to a 50-Ω system impedance; instead its S-parameters are referenced to the characteristic impedance Z_0 of the "native geometry" transmission lines attached to its ports. This method of solution is essentially identical to the Bosma [9] solution of 1965. Standard S-parameter matrix conversion formulas may now be applied to renormalize the intrinsic circulator to a different impedance or embed the circulator in a complex network. We may embed this solution into standard circuit simulators if we renormalize the reference impedance to 50 Ω (following, for example, [18]) and let the circuit simulator supply the embedding network. A natural design choice for an embedding network would be to embed the intrinsic circulator into a set of standardized quarter-wave matching structures. The resulting frequency response of the circulator circuit is due to the cascade of the intrinsic circulator performance with that of the impedance-matching network.

Fig. 9(a) and (b) shows, respectively, the measured insertion loss and isolation versus frequency, and measured return loss versus frequency, compared to calculations done with

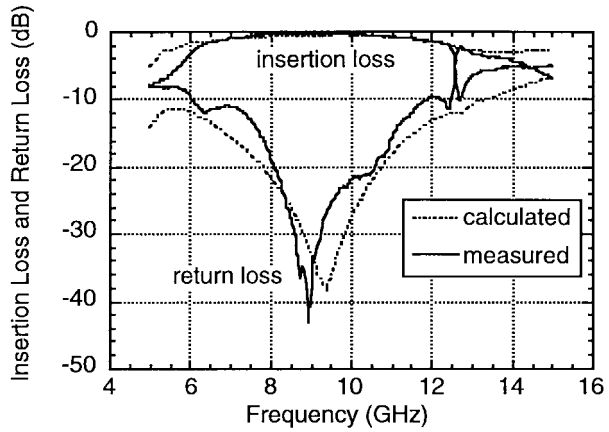

(a)

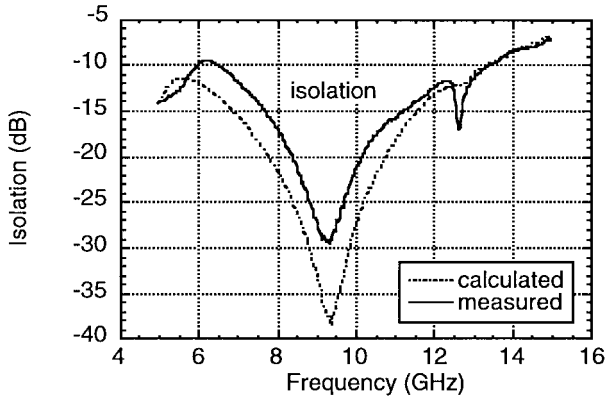

(b)

Fig. 9. Scattering parameters calculated with the RGF technique compared with measurement. The circulator is the same device that was simulated with the PDE2D code in Fig. 6(a). This device is a planar embedded puck design, in which the ferrite puck is contained entirely within a dielectric substrate. There are single-stage quarter-wave matching transformers ($f_{\text{center}} = 9.5$ GHz) attached to each port. (Fabricated by D. J. Popelka and G. Harrison of EMS Technologies, Inc, Norcross, GA, for the DARPA FDC).

the RGF code. Radial variation of the internal magnetic field H_{int} caused by demagnetization is taken into account. Comparison is made with experiment by using a computational port aperture width $w_c = 1.4w$ where w is the physical width of the circulator port microstrip lines. This correction to w must be made because of the fringing fields accompanying open microstrip structures [16], [17].

B. Solving for Electric Fields Inside the Puck

Once S_{11}, S_{21}, and S_{31} of the intrinsic circulator are obtained we can find the electric fields at an interior response point in terms of the incident electric field by substituting (37b), (37d), and (37f) into (33). The result is

$$E(r,\phi) = [G_1(1 - S_{11}) - G_2 S_{21} - G_3 S_{31}]\frac{E_1^{\text{inc}}}{Z_0} = L_1 E_1^{\text{inc}} = L_1\sqrt{Z_0}a_1 \tag{40}$$

and L_1 is the solution when the incident field is at port 1 only. This solution is plotted in Fig. 10(a) and compares excellently with the field pattern generated by the 2-D FE solution in

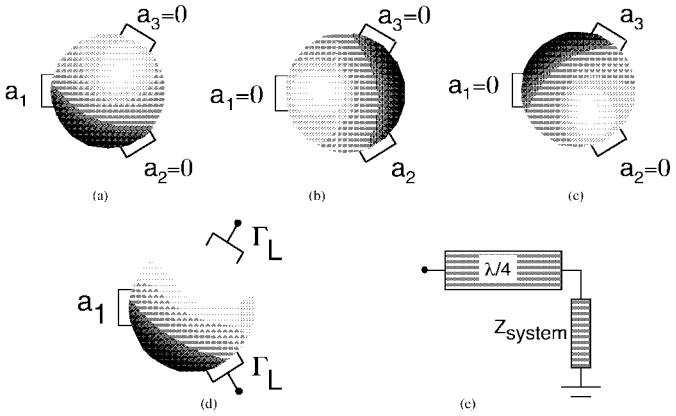

Fig. 10. Electric-field patterns for the intrinsic circulator and matched circulator calculated using the RGF technique at a frequency corresponding to maximum isolation. The patterns are calculated by assuming incident signals at (a) port 1 only, (b) port 2 only, and (c) port 3 only, with no incident signal at any of the other ports. The three patterns are weighted and superimposed in (d), assuming a unit incident signal at port 1 and signals at ports 2 and 3 weighted by the reflection coefficients obtained by terminating ports 2 and 3 in the matching network shown in (e). The darker regions of the contours correspond to higher electric fields, and the lighter regions to lower electric fields. When all three contributions to the total field are superimposed, the isolation at port 3 is clearly evident. [The device parameters are identical to those used in Fig. 6(a).]

Section II. Here we have made use of the fact that E^{inc} is a traveling electric-field wave in a microstrip transmission line of characteristic impedance Z_0, so we can write the electric field in the interior of the circulator in terms of the normalized transmission-line traveling-wave component

$$a_1 = \frac{E_1^{\text{inc}}}{\sqrt{Z_0}}. \tag{41}$$

By superposition we can obtain the total field when there is incidence at all three ports:

$$E(r,\phi) = (L_1 a_1 + L_2 a_2 + L_3 a_3)\sqrt{Z_0} \tag{42}$$

where L_2 and L_3 are electric-field distributions similar to L_1 except that they are rotated by $+$ and $-$ 120°, because they represent disk resonances excited by inputs at ports 2 and 3, respectively, rather than at port 1. Fig. 10(a)–(c) shows the field plots calculated by this technique for incidence at only one of the three ports of the circulator, each taken in turn.

To find the total field when terminations are placed at the ports, we only need to find a_2 and a_3 in terms of a_1. Suppose all ports have identical matching networks attached to them followed by a termination in the system impedance Z_{sys}. Let each matching network have the same symmetrical scattering matrix as follows:

$$[S^{\text{mn}}] = \begin{bmatrix} S_{11}^{\text{mn}} & S_{21}^{\text{mn}} \\ S_{21}^{\text{mn}} & S_{22}^{\text{mn}} \end{bmatrix} \tag{43}$$

with port 1 of the matching network attached to the system impedance and port 2 attached to the circulator. The load reflection coefficient looking outward from each of the circulator ports into the system-terminated matching network is

$$\Gamma_L = S_{22}^{\text{mn}} + \frac{\left(S_{21}^{\text{mn}}\right)^2 \Gamma_{\text{sys}}}{1 - S_{11}^{\text{mn}}\Gamma_{\text{sys}}} \tag{44}$$

where

$$\Gamma_{\rm sys} = \frac{Z_{\rm sys} - Z_0}{Z_{\rm sys} + Z_0}. \tag{45}$$

We now incorporate this loading into the circulator. Let $\alpha = S_{11}, \beta = S_{21}$, and $\gamma = S_{31}$ for the intrinsic circulator. Then

$$\begin{pmatrix} b_1 \\ b_2 \\ b_3 \end{pmatrix} = \begin{bmatrix} \alpha & \gamma & \beta \\ \beta & \alpha & \gamma \\ \gamma & \beta & \alpha \end{bmatrix} \begin{pmatrix} a_1 \\ a_2 \\ a_3 \end{pmatrix}. \tag{46}$$

The relations at ports 2 and 3 looking outward are $a_2 = \Gamma_L b_2$ and $a_3 = \Gamma_L b_3$. Substituting in the above equation, we obtain

$$\begin{pmatrix} b_1 \\ b_2 \\ b_3 \end{pmatrix} = \begin{bmatrix} \alpha & \gamma & \beta \\ \beta & \alpha & \gamma \\ \gamma & \beta & \alpha \end{bmatrix} \begin{pmatrix} a_1 \\ b_2\Gamma_L \\ b_3\Gamma_L \end{pmatrix} \tag{47}$$

or, rearranging

$$\begin{bmatrix} 1 & -\gamma\Gamma_L & -\beta\Gamma_L \\ 0 & 1-\alpha\Gamma_L & -\gamma\Gamma_L \\ 0 & -\beta\Gamma_L & 1-\alpha\Gamma_L \end{bmatrix} \begin{pmatrix} b_1 \\ b_2 \\ b_3 \end{pmatrix} = \begin{pmatrix} \alpha \\ \beta \\ \gamma \end{pmatrix} a_1. \tag{48}$$

We can solve this for the scattered waves b_1, b_2, and b_3 and, thereby, find the incident waves a_2 and a_3 in terms of a_1:

$$a_2 = \Gamma_L b_2 = K_2 a_1 = \Gamma_L \frac{\beta(1-\alpha\Gamma_L) + \gamma^2\Gamma_L}{(1-\alpha\Gamma_L)^2 - \beta\gamma\Gamma_L^2} a_1 \tag{49}$$

$$a_3 = \Gamma_L b_3 = K_3 a_1 = \Gamma_L \frac{\gamma(1-\alpha\Gamma_L) + \beta^2\Gamma_L}{(1-\alpha\Gamma_L)^2 - \beta\gamma\Gamma_L^2} a_1 \tag{50}$$

and

$$b_1 = (\alpha + \beta K_3 + \gamma K_2) a_1 = \Gamma_c a_1. \tag{51}$$

Here, Γ_c is the input reflection coefficient looking into port 1 referenced to Z_0 when the circulator is terminated at ports 2 and 3 with matching networks which are themselves terminated in the system impedance. K_2 and K_3 are convenient collections of terms from (49) and (50). We then have

$$E(r,\phi) = (L_1 + L_2K_2 + L_3K_3)\sqrt{Z_0}a_1. \tag{52}$$

If $|\alpha| \ll 1$, $|\gamma| \ll 1$, and $|\beta| \approx 1$, which is true for a well-designed circulator near the center of its band, then $K_2 \approx \beta\Gamma_L$ and $K_3 \approx \gamma\Gamma_L + (\beta\Gamma_L)^2$, so these coefficients approximately represent one-trip and two-trip reflections off of the matching structures at ports 2 and 3, respectively. Thus, K_2 is small and K_3 is even smaller. This means the electric-field pattern in the circulator when matched will look a lot like the intrinsic pattern L_1, but with corrections given by the complex amplitudes of K_2 and K_3.

The field patterns for the matched circulator calculated using this technique are shown in Fig. 10(d). The way in which the field pattern depends on frequency for the matched circulator is shown in Fig. 11. The ferrite disk resonator exhibits a null in the standing-wave electric field, whose location and behavior determines the isolation. As frequency is increased, the null travels around the perimeter of the circulator in a clockwise direction. At the circulation frequency, the null is located at the isolated port. The spatial width of the null and the rate at which it traverses the port aperture with frequency determines the bandwidth of the circulator. At high frequencies, the resonance in the puck breaks up into a higher order mode.

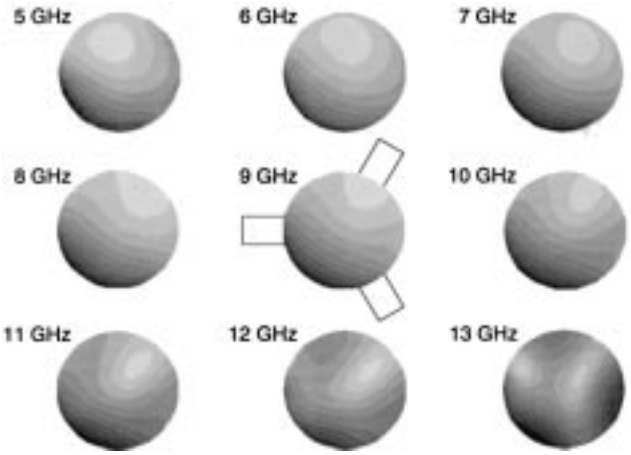

Fig. 11. Frequency sweep of the contours of constant electric field in the matched round circulator calculated by the RGF technique of Fig. 10(d). The input port is at the left of the disk and the isolated port is at the upper right of the disk. The darker regions of the contours correspond to higher electric fields, and the lighter regions to lower electric fields, and the ports are indicated on the middle diagram. These plots indicate that the null in the signal proceeds around the perimeter of the puck, moving clockwise with frequency. The minimum signal at port 3 and maximum isolation occur near 9.5 GHz. Above 12 GHz, the field pattern in the puck breaks up into a higher order resonance.

We may relate these field plots quantitatively to the incident power as follows. The incident wave a_1 may be found in terms of a_0, the wave incident on the matching network in front of port 1. It is given by

$$a_1 = \frac{S_{21}^{\rm mn}}{1 - S_{22}^{\rm mn}\Gamma_c} a_0 \tag{53}$$

so that

$$E(r,\phi) = (L_1 + L_2K_2 + L_3K_3)\sqrt{Z_0}\frac{S_{21}^{\rm mn}}{1 - S_{22}^{\rm mn}\Gamma_c} a_0. \tag{54}$$

Finally, the incident wave a_0 can be related to the incident power by $a_0 = \sqrt{2P_{\rm inc}}$, yielding

$$E(r,\phi) = (L_1 + L_2K_2 + L_3K_3)\frac{S_{21}^{\rm mn}}{1 - S_{22}^{\rm mn}\Gamma_c}\sqrt{2Z_0P_{\rm inc}}. \tag{55}$$

Equation (55) gives the field at every point in the circulator, as a function of the RF power incident on the input to the matching structure.

IV. Conclusion

We have shown applications of circulator analysis by two techniques—a 2-D FE technique and an RGF technique. The 2-D FE method is shown to solve for the distribution of internal magnetic field inside a round ferrite puck, and has been shown to verify the usefulness of analytical expansions which have existed in the literature to account for the demagnetizing fields in finite-sized pucks. The 2-D FE method has also been used to calculate the RF fields and scattering parameters in circulators having noncircular shapes, and can easily and naturally be adapted to analyze a circulator having nonuniform material properties. The 2-D FE codes

used here run much slower than analytical codes, taking several minutes per frequency point. We have also investigated the field solutions for round circulators calculated using the RGF technique. This technique allows for radially varying properties in the material or bias fields, and is limited to round devices. Results of the RGF technique are compared to measurements on an embedded puck circulator. We have shown how the impedance-matching structures attached to the circulator affect the field distributions inside, and plotted the behavior of the field distributions with frequency. The field plots have provided insight into the nature of the ferrite puck resonance which creates circulation.

ACKNOWLEDGMENT

The authors would like to thank the participants of the DARPA FDC, particularly R. E. Neidert, for illuminating discussions throughout this effort, and D. J. Popelka and G. Harrison of EMS Technologies, Inc., Norcross, GA, for fabricating the embedded puck circulator used in the measurements.

REFERENCES

[1] B. Hershenov, "X-band microstrip circulator," *Proc. IEEE*, vol. 54, pp. 2022–2023, Dec. 1966.
[2] C. M. Williams, D. B. Chrisey, P. Lubitz, K. S. Grabowski, and C. M. Cotell, "The magnetic and structural properties of pulsed laser deposited epitaxial MnZn-ferrite films," *J. Appl. Phys.*, vol. 75, pp. 1676–1680, Feb. 1994.
[3] J. D. Adam, H. Buhay, M. R. Daniel, G. W. Eldridge, M. H. Hanes, R. L. Messham, and T. J. Smith, "K-band circulators on semiconductor wafers," in *IEEE MTT-S Int. Microwave Symp. Dig.*, San Francisco, CA, June 1996, pp. 113–115.
[4] G. Sewell. (1993). "PDE2D: Easy-to-use software for general two-dimensional partial differential equations," *Advances in Engineering Software*, (vol. 17), pp. 105–112. Available: URL: http://members.aol.com/pde2d, or Granville Sewell, P.O. Box 12141, El Paso, TX 79913.
[5] G. Sewell and S. R. Cvetkovic, "WAVEGIDE—An interactive waveguide program," in *Advances in Engineering Software*, vol. 11., 1989, pp. 169–175.
[6] S. R. Cvetkovic, A. P. Zhao, and M. Punjani, "An implementation of the finite-element analysis of anisotropic waveguides through a general-purpose PDE software," *IEEE Trans. Microwave Theory Tech.*, vol. 42, pp. 1499–1505, Aug. 1994.
[7] *Microwave Materials: A Technical Supplement*, Trans-Tech, Inc., Adamstown MD, Pub. 500301 R1, 1989.
[8] R. I. Joseph and E. Schloemann, "Demagnetizing field in nonellipsoidal bodies," *J. Appl. Phys.*, vol. 36, pp. 1579–1593, May 1965.
[9] H. Bosma, "On stripline Y-circulation at UHF," *IEEE Trans. Microwave Theory Tech.*, vol. MTT-12, pp. 61–72, Jan. 1964.
[10] C. M. Krowne and R. E. Neidert, "Theory and numerical calculations for radially inhomogeneous circular ferrite circulators," *IEEE Trans. Microwave Theory Tech.*, vol. 44, pp. 419–431, Mar. 1996.
[11] B. Lax and K. J. Button, *Microwave Ferrites and Ferrimagnetics*. New York: McGraw-Hill, 1962, pp. 150–151.
[12] R. E. Neidert, "Computer aided approach to the design of Y-junction stripline and microstrip ferrite circulators," Naval Res. Lab., Washington, D.C., Rep. NRL/FR/6851-92-9381, May 1992.
[13] R. E. Neidert and P. M. Phillips, "Losses in Y-junction stripline and microstrip ferrite circulators," *IEEE Trans. Microwave Theory Tech.*, vol. 41, pp. 1081–1086, June/July 1993.
[14] C. M. Krowne, "Theory of the recursive Green's function for inhomogeneous ferrite canonically shaped microstrip circulators," in *Advances in Imaging and Electron Physics*, vol. 98, Peter W. Hawkes, Ed. New York: Academic, 1996.
[15] C. M. Krowne, "3-D dyadic Green's function for radially inhomogeneous circular ferrite circulator," in *IEEE MTT-S Int. Microwave Symp. Dig.*, San Francisco, CA, June 1996, pp. 121–124.
[16] H. S. Newman, D. C. Webb, and C. M. Krowne, "Design and realization of millimeter-wave microstrip circulators," in *Proc. Int. Conf. Millimeter Submillimeter Waves Applicat. III*, SPIE, Denver, CO, Aug. 1996, pp. 181–191.
[17] J. T. Vaughn, D. J. Popelka, and S. T. Williams, "Application of CAD tools for planar ferrite circulators," presented at the IEEE MTT-S Int. Symp. Workshop Ferrite CAD Applicat., San Francisco, CA, June 17, 1996.
[18] K. Kurokawa, "Power waves and the scattering matrix," *IEEE Trans. Microwave Theory Tech.*, vol. MTT-13, pp. 194–202, Mar. 1965.

Harvey S. Newman (S'72–M'80) received the B.S. degree from Northwestern University, Evanston, IL, in 1973, and the M.S. and Ph.D. degrees from the University of Wisconsin-Madison, in 1975 and 1980, respectively, all in electrical engineering.

In 1980, he joined the Microwave Technology Branch, Electronics Science and Technology Division, Naval Research Laboratory, Washington, DC, where he has been responsible for basic and applied research on microwave and millimeter-wave components. He has authored or co-authored numerous conference and journal papers on superconducting transmission lines, cryogenic bolometers, heterostructure devices, and high-Tc superconducting resonator measurements, and high-Tc superconducting microwave filters. More recently, he has been investigating optical techniques for measuring the spatial profile of the microwave current density on planar superconducting transmission lines. He holds two patents and has given several invited talks and workshops. From 1993 to 1995, he participated in the DARPA-sponsored FDC, for which he investigated analytical and FE numerical methods applied to the CAD of thin-film ferrite circulators, lumped-element circulators, and magnetostatic-wave ferrite filters.

Dr. Newman is a member of the American Physical Society and the IEEE Microwave Theory and Techniques Society. He has served on the 1985 MTT-S Adcom Nominations Committee, and the 1998 IEEE MTT-S International Microwave Symposium Technical Program Steering Committee.

Clifford M. Krowne (S'73–M'74–SM'83) received the B.S. degree from the University of California at Berkeley, in 1970, the M.S. degree from the University of California at Davis, in 1972, and Ph.D. degree from University of California at Los Angeles, in 1975.

He has worked in the Microelectronics Division, Lockheed Missiles and Space Company, Sunnyvale, CA, as a Member of the Solid-State Technical Staff, Watkins-Johnson Company, Palo Alto, CA, and as a Faculty Member in the Department of Electrical Engineering, North Carolina State University, Raleigh. Since 1982, he has been with the Microwave Technology Branch, Electronics Science and Technology Division, Naval Research Laboratory, Washington, DC, studying microwave and millimeter-wave properties of active and passive solid-state devices. He also was an Adjunct Professor of electrical engineering at the University of Maryland at College Park. He has authored or co-authored 144 conference papers, books, and journal papers and holds several patents on solid-state electronics, microwave circuits, electromagnetics, engineering education, and applied physics. He has also authored the major portions of two books for Academic Press in the Advances in Imaging and Electron Physics series (vol. 92, 1995; vol. 98, 1996).

Dr. Krowne is a member of Phi Kappa Phi and Tau Beta Pi, and is a Fellow of the Washington Academy of Sciences. He has served on the technical program conference committees of the IEEE Antennas and Propagation Society (1983, 1984) and the IEEE Microwave Theory and Techniques Society (1982–1996), has chaired sessions in the electromagnetic theory, microstrip antenna, and solid-state devices/circuits, superconductor, and monolithic circuit areas, and has organized two MTT-S workshops on 2-D/3-D full-wave simulation (1992), and self-consistent particle transport/full-wave dynamic field simulation (1993). He was a member of the 1987 IEEE Microwave Theory and Techniques Symposium Steering Committee. He is listed in *Who's Who in Frontiers of Science and Technology* and *Who's Who in Electromagnetics*.